The current issue and full text archive of this journal is available at
www.emeraldinsight.com/0961-5539.htm

Natural convection heat transfer augmentation in a partially heated and partially cooled square cavity utilizing nanofluids

Manab Kumar Das
Department of Mechanical Engineering, Indian Institute of Technology Kharagpur, Kharagpur, India, and
Pravin Shridhar Ohal
Tata Motors, Pune, India

Received 22 May 2007
Revised 2 January 2008
Accepted 28 January 2008

Abstract

Purpose – The purpose of this paper is to investigate the behaviour of nanofluids numerically inside a partially heated and partially cooled square cavity to gain insight into heat transfer and flow processes induced by a nanofluid.

Design/methodology/approach – A model is developed to analyze the behaviour of nanofluids taking into account the solid volume fraction χ. The transport equations are solved numerically with finite volume approach using SIMPLEC algorithm.

Findings – Comparisons with previously published work on the basis of special cases are performed and found to be in excellent agreement. Five different relative positions of the active zones are considered.While circulation depend strongly on the total exit length. Governing parameters were $10^3 < Gr < 10^7$ but due to space constraints the results for $10^4 < Gr < 10^7$ are presented. It is found that both the Grashof number and solid volume fraction χ affect the fluid flow and heat transfer in the cavity. CopperWater nanofluid is used with $Pr = 6.2$ and solid volume fraction is varied as 0, 4, 8, 12, 16 and 20 per cent. Detailed results are presented for flow pattern and heat transfer curves.

Originality/value – The present study focusses on the analysis of several parameters on the heat transfer characteristics of nanofluids within the enclosure.

Keywords Flow, Convection, Heat transfer, Nanotechnology
Paper type Research paper

Nomenclature

k_f	thermal conductivity of the fluid (W/m K)
k_s	thermal conductivity of the solid (W/m K)
Nu	local Nusselt number
$\overline{Nu}$	average Nusselt number
Pr	Prandtl number (ν_f/α_f)
Gr	Grashoff number for the fluid
u^*, v^*	dimensional velocity components along (x^*, y^*) axes (m/s)
u, v	dimensionless velocity components along (x, y) axes
x^*, y^*	dimensional Cartesian co-ordinates (m)
x, y	dimensionless Cartesian co-ordinates

Greek symbols

α	thermal diffusivity (m^2/s)
β_f	fluid thermal expansion coefficient (K^{-1})
β_s	solid expansion coefficient (K^{-1})
κ	excess thermal conductivity enhancement coefficient
ν	kinematic viscosity (m^2/s)
χ	solid volume fraction

International Journal of Numerical Methods for Heat & Fluid Flow
Vol. 19 Nos. 3/4, 2009
pp. 411-431

0961-5539
DOI 10.1108/09615530910938353

Subscripts

c	cold wall
eff	effective
f	fluid
h	hot wall
nf	nanofluid
o	reference value
s	solid

Superscript

*	dimensional term

1. Introduction

In case of natural convection, there is a low heat transfer because of the low thermal conductivity of the conventional heat transfer fluids such as water, oil and ethylene glycol mixture. This limitation may be overcome by suspending very fine particles with relatively high thermal conductivity and thus enhance the heat transfer rate. The advanced heat transfer fluid thus developed is referred to as a nanofluid (Eastman *et al.*, 2001). It possesses a substantially larger thermal conductivity compared to that of the traditional fluids. The presence of the nanoparticles in the fluids increases appreciably the effective thermal conductivity of the fluid and consequently enhances the heat transfer characteristics.

The natural convection problem in a differentially heated two-dimensional square cavity is numerically simulated by Khanafer *et al.* (2003) considering the solid particle dispersion effect. In their methodology, the dispersion constant "C" is to be determined by experimental data observation. A heat transfer correlation of the average Nusselt number for various Grashof numbers (*Gr*) and volume fractions is presented. Using different correlations analytically, Chein and Huang (2005) have analyzed microchannel heat sink performance using nanofluids as coolants. They have reported the Nusselt number and pressure drop based on Reynolds number and pumping power. Koo and Kleinstreuer (2005) have used Brownian motion based-thermal conductivity and viscosity to numerically simulate the microheat sink. Additionally they have considered the viscous dissipation term. They suggested that a high-Prandtl number base fluid and a high aspect ratio channel should be used for better heat transfer performance.

Valencia and Frederick (1989) have numerically studied the natural convection of air in square cavities with half-active and half-insulated vertical walls for Rayleigh numbers of 10^3–10^7. Five different relative positions of the active zones are considered. Expressions for average Nusselt number in the five situations are given as empirical correlations. Recently, Tiwari and Das (2007) have investigated the behaviour of nanofluids numerically inside a two-sided lid-driven differentially heated square cavity to gain insight into convective recirculation and flow processes induced by a nanofluid. The left and the right moving walls are maintained at different constant temperatures while the upper and the bottom walls are thermally insulated. Three case were considered depending on the direction of the moving walls. CopperWater nanofluid is used with $Pr = 6.2$ and solid volume fraction is varied as 0.0, 8, 16 and 20 per cent.

To investigate the heat transfer enhancement by very fine particles suspended in a fluid, a single-phase model is considered where both the fluid phase and the solid particles are in thermal equilibrium state and flow with the same local velocity. While studying the heat transfer enhancement utilizing nanofluids, the issues involved are like gravity, Brownian motion, layering at the interface between solid and liquid, clustering of the nanoparticles, ballistic phono transport through the particles and the friction between the fluid and the solid particles. The phenomena of sedimentation, dispersion and Brownian diffusion may coexist in the main flow of a nanofluid. If the

main interest is focused on the heat transfer process, the modified single-phase, accounting for some of the above factors, is more convenient than a two-phase model. The superior characteristics of the nanofluid allow it to behave more like a fluid rather than the conventional solid–fluid mixtures. In the present case, modeling the effective thermal conductivity poses a challenge while studying the heat transfer enhancement. Maxwell's model (Maxwell, 1904) predicted that the effective thermal conductivity of suspensions containing spherical particles increases with an increase in the volume fraction of the solid particles. Hamilton and Crosser (1962) have given an expression for the effective thermal conductivity of two-component mixtures taking into consideration the liquid and solid particle thermal conductivities, particle volume fraction and an empirical scaling factor to account for the different shapes of the particles.

Natural convection problem in enclosures are encountered in a variety of engineering applications especially for cooling of electronic components, solar energy collection, etc. Natural convection configuration is encountered where the left and the right walls are partially heated and partially cooled and the remaining perimeter is insulated. The present study is based on such a configuration. The present study is focussed on the analysis of several pertinent parameters on the heat transfer characteristics of nanofluids within the enclosure. In the present study, a steady-state incompressible flow solver has been applied for simulating the flow features of nanofluids for a range of solid volume fraction (χ) values and *Gr*.

2. Mathematical formulation

Consider a square cavity filled with a nanofluid. The vertical walls are partially heated and partially cooled, the remaining portion of the vertical walls and the horizontal walls are assumed to be insulated, non-conducting and impermeable to mass transfer. Half the height of the right-hand wall is kept at a temperature T_h. Also half the height of the left-hand wall is at temperature T_c, $T_h > T_c$. The remaining part of the perimeter are insulated. Five different cases were considered as shown in Figure 1 based on the position of the hot and the cold region. In Case I (Figure 1(a)), the hot region is located at the bottom and the cold region at the top of their respective walls. In Case II (Figure 1(b)), the hot and the cold regions are at the top right and at the bottom left regions, respectively. In Cases III (Figure 1(c)) and IV (Figure 1(d)), both the active sections are directly opposite to each other, at the lower half of the enclosure and at an intermediate position, respectively. Finally, in Case V (Figure 1(e)), the hot region is located at the right-hand wall from $y = 0.25$ to 0.75 whereas the cold region occupies the bottom half of the left-hand wall. The nanofluid in the enclosure is Newtonian, incompressible and laminar. The nanoparticles are assumed to have a uniform shape and size. Moreover, it is assumed that both the fluid phase and nanoparticles are in thermal equilibrium state and they flow at the same velocity. The thermophysical properties of the nanofluid are assumed to be constant except for the density variation in the buoyancy force, which is based on the Boussinesq approximation.

The continuity, momentum and energy equations are considered for a Newtonian, Fourier constant property fluid governing a steady, two-dimensional flow. It is further assumed that radiation heat transfer among sides is negligible with respect to other modes of heat transfer. Under the assumption of constant thermal properties, the Navier-Stokes equation for an steady, incompressible, two-dimensional flow are

Continuity equation:

$$\frac{\partial u^*}{\partial x^*} + \frac{\partial v^*}{\partial y^*} = 0 \tag{1}$$

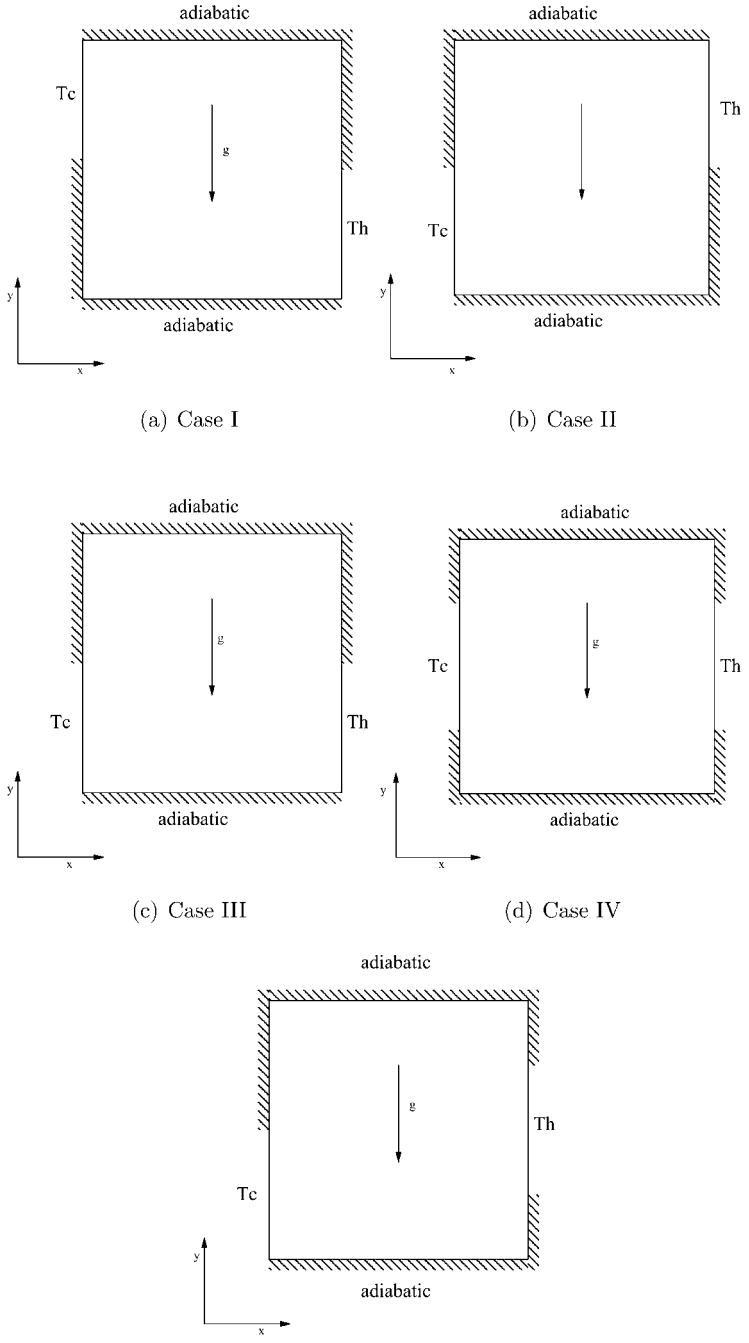

Figure 1.
Physical model for five cases and the coordinate system

x-momentum equation:

$$\frac{\partial(u^{*2})}{\partial x^*}+\frac{\partial(u^*v^*)}{\partial y^*}=-\frac{1}{\rho_{nf,o}}\frac{\partial p^*}{\partial x^*}+\frac{\mu_{eff}}{\rho_{nf,o}}\left(\frac{\partial^2 u^*}{\partial x^{*2}}+\frac{\partial^2 u^*}{\partial y^{*2}}\right) \tag{2}$$

y-momentum equation:

$$\frac{\partial(u^*v^*)}{\partial x^*}+\frac{\partial(v^{*2})}{\partial y^*}=-\frac{1}{\rho_{nf,o}}\frac{\partial p^*}{\partial y^*}+\frac{\mu_{eff}}{\rho_{nf,o}}\left(\frac{\partial^2 v^*}{\partial x^{*2}}+\frac{\partial^2 v^*}{\partial y^{*2}}\right)+\frac{1}{\rho_{nf,o}}[\chi\rho_{s,o}\beta_s+(1-\chi)\rho_{f,o}\beta_f]g(T-T_c) \tag{3}$$

Energy equation:

$$\frac{\partial(u^*T^*)}{\partial x^*}+\frac{\partial(v^*T^*)}{\partial y^*}=\alpha_{nf}\left(\frac{\partial^2 T^*}{\partial x^{*2}}+\frac{\partial^2 T^*}{\partial y^{*2}}\right) \tag{4}$$

where:

$$\alpha_{nf}=k_{eff}/(\rho C_p)_{nf,o}$$

The viscosity of the nanofluid can be estimated with the existing relations for the two-phase mixture. The equation given by Brinkman (1952) has been used as the relation for effective viscosity in this problem, as given by

$$\mu_{eff}=\frac{\mu_f}{(1-\chi)^{2.5}} \tag{5}$$

Xuan and Li (1999) have experimentally measured the apparent viscosity of the transformer oil–water nanofluid and of the water–copper nanofluid in the temperature range of 20-50°C. The experimental results reveal relatively good agreement with Brinkman's theory.

The effective density of the nanofluid at reference temperature is

$$\rho_{nf,o}=(1-\chi)\rho_{f,o}+\chi\rho_{s,o} \tag{6}$$

and the heat capacitance of nanofluid is

$$(\rho C_p)_{nf}=(1-\chi)(\rho C_p)_f+\chi(\rho C_p)_s \tag{7}$$

as given by Xuan and Li (2003). The effective thermal conductivity of fluid can be determined by Maxwell–Garnett's (MG model) self-consistent approximation model. For the two-component entity of spherical–particle suspension, the MG model gives

$$\frac{k_{eff}}{k_f}=\frac{(k_s+2k_f)-2\chi(k_f-k_s)}{(k_s+2k_f)+\chi(k_f-k_s)} \tag{8}$$

In the absence of any convenient formula, the calculation of effective thermal conductivity can be obtained from the above equation. For further analysis, it is convenient to introduce the excess thermal conductivity enhancement coefficient κ, defined as

$$\kappa = \frac{k_{eff} - k_f}{k_{HC} - k_f} \tag{9}$$

In the above definition, κ is simply the ratio of measured thermal conductivity increase divided by the increase predicted by the Hamilton–Crosser (HC) theory. Consequently, $\kappa = 1$ indicates agreement with the macroscopic theory, and $\kappa > 1$ measures the magnitude of thermal-conductivity enhancement. The above equations can be converted to non-dimensional form, using the following dimensionless parameters

$$x = \frac{x^*}{H} \quad y = \frac{y^*}{H} \quad u = \frac{u^* H}{\alpha} \quad v = \frac{v^* H}{\alpha} \quad p = \frac{p^* H^2}{(\rho_{nf,o}) \cdot \alpha^2}$$
$$T = \frac{T^* - T_c^*}{\Delta T^*} \quad Gr = \frac{g\beta H^3 \Delta T^*}{\nu_f^2} \quad Pr = \frac{\nu_f}{\alpha_f}$$

The governing equations can now be written in dimensionless form as follows

Continuity equation:

$$\frac{\partial u}{\partial x} + \frac{\partial v}{\partial y} = 0 \tag{10}$$

x-momentum equation:

$$\frac{\partial (u^2)}{\partial x} + \frac{\partial (uv)}{\partial y} = -\frac{\partial p}{\partial x} + Pr \frac{\rho_{f,o}}{\rho_{nf,o}} \frac{1.0}{(1-\chi)^{2.5}} \left(\frac{\partial^2 u}{\partial x^2} + \frac{\partial^2 u}{\partial y^2} \right) \tag{11}$$

y-momentum equation:

$$\frac{\partial (uv)}{\partial x} + \frac{\partial v^2}{\partial y} = -\frac{\partial p}{\partial y} + Pr \frac{\rho_{f,o}}{\rho_{nf,o}} \frac{1.0}{(1-\chi)^{2.5}} \left(\frac{\partial^2 v}{\partial x^2} + \frac{\partial^2 v}{\partial y^2} \right) + GrPr^2 \frac{\rho_{f,o}}{\rho_{nf,o}} \left[1 - \chi + \chi \frac{\rho_s \beta_s}{\rho_f \beta_f} \right] \tag{12}$$

Energy equation:

$$\frac{\partial (uT)}{\partial x} + \frac{\partial (vT)}{\partial y} = \frac{k_{eff}}{k_f} \frac{(\rho Cp)_f}{(\rho Cp)_{nf}} \left[\frac{\partial^2 T}{\partial x^2} + \frac{\partial^2 T}{\partial y^2} \right] \tag{13}$$

Boundary conditions are $u = 0$ and $v = 0$ on all four walls. All thermal boundary conditions are adiabatic $(\partial T/\partial n) = 0$ except for those of the hot and cold plate where $T_h = 1$ and $T_c = 0$, respectively.

The Nusselt number of the nanofluids is expected to depend on a number of factors such as thermal conductivity and heat capacitance of both the pure fluid and the

ultrafine particles, the volume fraction of the suspended particles, the flow structure and the viscosity of the nanofluid. The local variation of the Nusselt number of the nanofluid can be expressed as:

$$Nu = \frac{Q}{Q_{cond,fluid}} = -\frac{(k_{eff})_{stagnant}}{k_f}\frac{\partial T}{\partial X} \tag{14}$$

where

$$Q = -(k_{eff})_{stagnant} A \frac{\partial T^*}{\partial x^*}|_{x^*=0} \tag{15}$$

The average Nusselt number along the Right wall is calculated by integrating the local Nusselt number over the Right wall.

$$\overline{Nu} = \frac{1}{L}\int_0^1 Nu\, dy \tag{16}$$

3. Numerical procedure

The governing equations are solved numerically by finite-volume method with staggered gird arrangement. The *s*emi *i*mplicit *m*ethod for *p*ressure *l*inked *e*quation *c*onsistent (SIMPLEC) (Van Doormaal and Raithby, 1984) is used to couple the momentum and the continuity equations. The third order accurate deferred QUICK scheme of Hayase *et al.* (1990) is employed to minimize the numerical diffusion for the convective terms for both the momentum equations and the energy equation. The solution of the discretized momentum and pressure correction equation is obtained by TDMA line-by-line method (Patankar, 1980). The iterative procedure is initiated by the solution of momentum equations followed by energy equation and is continued until convergence is achieved. Euclidean norm of the residual is taken as convergence criteria for each dependent variable in the entire flow field (Van Doormaal and Raithby, 1984). The mass balance for convergence was taken as 10^{-7}.

4. Validation of the code

The problem of a two-dimensional lid-driven square-cavity flow problem (Ghia *et al.*, 1982) has been solved and compared. Then the present code is validated for natural convection heat transfer in a square cavity with differentially heated side walls. The left wall was kept hot while the right wall was cooled whereas the top and the bottom walls are insulated. Table I compares the results with those by de Vahl Davis (1983), Markatos and Pericleous (1984), and Hadjisophocleous *et al.* (1998), Fusegi *et al.* (1991) and Ha and Jung (2000). The computed results are in very good agreement with the benchmark solution. The natural convection problem in a differentially heated square enclosure using nanofluids has been solved and compared the results with those of Santra *et al.* (2004) (Figure 2). A very good agreement has been obtained. Khanafer *et al.* (2003) have also solved the same problem with dispersion model. However, the value of constant "C" is not given. So the dispersion model has not been used in the present case though the results have shown almost same pattern (not shown here).

	a[a]	b[b]	c[c]	d[d]	e[e]	f[f]	$((a–d)/a) * 100$
(a) $Ra = 10^3$							
u_{max}	3.649	3.544	3.544	3.6512			−0.0602
y	0.813	0.832	0.814	0.805			
v_{max}	3.697	3.593	3.586	3.6939			0.0838
x	0.718	0.168	0.186	0.1780			
$\overline{Nu}$	1.118	1.108	1.141	1.118	1.085	1.072	0.0
Nu_{max}	1.505	1.496	1.540	1.5089			−0.2632
y	0.092	0.0825	0.142	0.09322			
Nu_{min}	0.692	0.720	0.727	0.6904			0.2321
y	1.0	0.9925	0.991	0.9915			
(b) $Ra = 10^4$							
u_{max}	16.178	16.18	15.995	16.1659			0.0747
y	0.823	0.832	0.814	0.822			
v_{max}	19.617	19.44	18.894	19.5428			0.3782
x	0.119	0.113	0.103	0.1271			
$\overline{Nu}$	2.243	2.201	2.29	2.251	2.100	2.070	−0.3566
Nu_{max}	3.528	3.482	3.84	3.5544			−0.7482
y	0.143	0.1425	0.141	0.1440			
Nu_{min}	0.586	0.643	0.670	0.584			0.3412
y	1.0	0.9925	0.991	0.9915			
(c) $Ra = 10^5$							
u_{max}	34.73	35.73	37.144	34.4973			0.67
y	0.855	0.857	0.855	0.8559			
v_{max}	68.59	169.08	68.91	68.3965			0.2821
x	0.066	0.067	0.061	0.05932			
$\overline{Nu}$	4.519	4.430	4.964	4.5656	4.361	4.464	−1.031
Nu_{max}	7.117	7.626	8.93	7.9366			−11.51
y	0.081	0.0825	0.080	0.0762			
Nu_{min}	0.729	0.824	1.01	0.7228			0.8504
y	1.0	0.9925	1.0	0.9915			
(d) $Ra = 10^6$							
u_{max}	64.63	68.81	66.42	65.7948			−1.8022
y	0.850	0.872	0.897	0.855			
v_{max}	217.36	221.8	226.4	219.1234			−0.8112
x	0.0379	0.0375	0.0206	0.04237			
$\overline{Nu}$	8.799	8.754	10.39	9.0821			−3.2174
Nu_{max}	17.925	17.872	21.41	19.3006			−7.6741
y	0.0378	0.0375	0.030	0.02542			
Nu_{min}	0.989	1.232	1.58	0.9495			4.7522
y	1.0	0.9925	1.0	0.9915			

Table I.
Comparison of solutions for natural convection in an enclosed cavity

Notes: [a]de Vahl Davis (1983), [b]Markatos and Perikleous (1984), [c]Hadjisophocleous *et al.* (1998), [d]present solution, [e]Fusegi *et al.* (1991), [f]Ha and Jung (2000)

5. Grid independence study

The grid independence test is performed using successively sized grids, 21 × 21, 41 × 41, 61 × 61 and 81 × 81 for Case I, $Gr = 10^7$ and $\chi = 20$ per cent. Uniform grid has been used for all the computations. The distribution of the u-velocity in the vertical mid-plane and temperature in the horizontal mid-plane are shown in Figure 3. It is observed that the curves overlap with each other for 61 × 61 and 81 × 81. So a grid

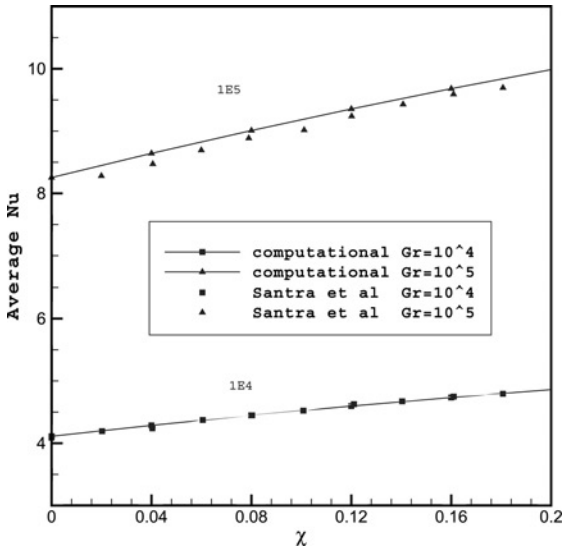

Figure 2.
Validation of the present code with the results of Santra *et al.* (2004)

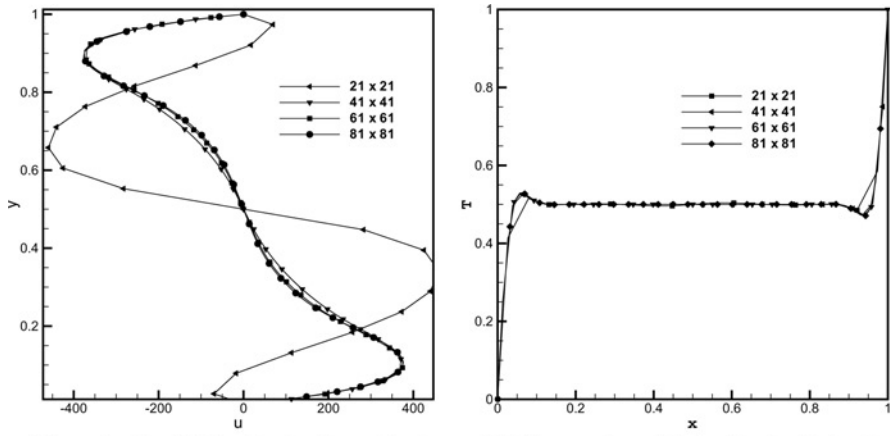

(a) u-velocity distribution in the vertical mid-plane

(b) Temperature distribution in the horizontal mid-plane

Figure 3.
Grid independence test for Case I, $Gr = 10^7$ and $\chi = 20$ per cent

number of 61×61 is chosen for further computation. Similar type of grid independence study has been carried out for other cases and are not reported here.

6. Results and discussion

The flow field, temperature field and heat transfer in a partially heated and partially cooled square cavity filled with nanofluid are examined. Five different cases are considered based on the active wall positions. The numerical code developed in the present investigation is used to carry out a number of simulations for a wide range of the controlling parameters of Gr and χ. The range of Gr for this investigation is varied between $10^3 < Gr < 10^7$. The range of χ used in this study is varied between $0 < \chi < 20$ per cent. The thermophysical properties of fluid and the solid phases are shown in Table II.

6.1 Streamline and isotherm distributions

It has been shown earlier (Tiwari and Das, 2007) that at low *Gr*, conduction is the mode of heat transfer. For high *Gr*, a strong convection is set in and thus the heat transfer increases. The representative streamline and isotherms for $Gr = 10^6$ for the five cases are shown in Figures 4-8. In Case I, for $\chi = 20$ per cent, as *Gr* increases the central vortex tends to become elliptic for $Gr = 10^4$ (not shown), and eventually breaks up into two vortices for $Gr = 10^5$ (not shown). The number of vortices formed are three for $Gr = 10^6$, and with further increase to $Gr = 10^7$ (not shown), the number of vortices formed are four in number. For $Gr = 10^6$, with the increase in χ the two small vortices ($\chi = 0.0$, Figure 4(a)) adjacent to the two primary vortices come closer at ($\chi = 4$ per cent, Figure 4(b)). They merge at ($\chi = 8$ per cent, Figure 4(c)) and with further increase in solid volume fraction at ($\chi = 12$ per cent, Figure 4(d)) they are now completely merged forming an elliptic single third vortex at $\chi = 16$ per cent (Figure 4(e)) and at $\chi = 20$ per cent (Figure 4(f)). The centers of two primary vortices tend to move towards each other with the increase in solid volume fraction. In all cases, at low *Gr*, the fluid rotates around the cavity midpoint. For all *Gr*, the thermal boundary layer goes on thinning with the increase of solid volume fraction (Figures 4(g)-4(l)).

In Case II, the effect of solid volume fraction on the streamlines and isotherms for *Gr* 10^6 is shown in Figure 5. For $Gr = 10^6$, with the increase in χ, the two vortices grow in size. In this case, the boundary layer starts at $y = 0.5$. The flow out of the active regions is subject to severe restriction imposed by the horizontal walls. Because of this, most of the fluid recirculates within the upper or lower halves of the enclosure, with only a weak circulation between the two halves. This pattern results in much weaker flow than in the preceding case.

In Case III, the effect of solid volume fraction on the streamlines and isotherms for $Gr = 10^6$ is shown in Figure 6. For $\chi = 20$ per cent, as *Gr* increases, the central vortex moves downward, towards the hot wall for $Gr = 10^4$ (not shown). It breaks up into two vortices for $Gr = 10^5$ (not shown), the centers of two vortices spread away from each other. Two vortices become approximately the same size for $Gr = 10^6$. Their center of rotation moves towards the active walls. In this case, the boundary layer forms at the lower half of the cavity. The flow in the upper half does not have the boundary layer characteristics. One of the boundary layers start at the corner while the other starts at $y = 0.5$. The fluid in the boundary layer on the hot side is free to move upwards from the end of the hot section, while the stream parallel to the opposite wall faces the restriction of a horizontal wall.

In Case IV, the effect of solid volume fraction on the streamlines and isotherms for $Gr = 10^6$ is shown in Figure 7. For $Gr = 10^6$, with the increase in χ, the secondary vortiex formed will grow and get separated at $\chi = 8$ per cent. With further increase in χ the center of two primary vortices come closer and small vortices will be merged with them at $\chi = 20$ per cent. The flow leaving an active wall region is free to move either upward or downwards.

Table II. Thermophysical properties of different phases

Property	Fluid phase (water)	Solid phase (copper)
c_p (J/kgK)	4,179	383
ρ (kg/m^3)	997.1	8,954
k (W/mK)	0.6	400
β (K^{-1})	2.1×10^{-4}	1.67×10^{-5}

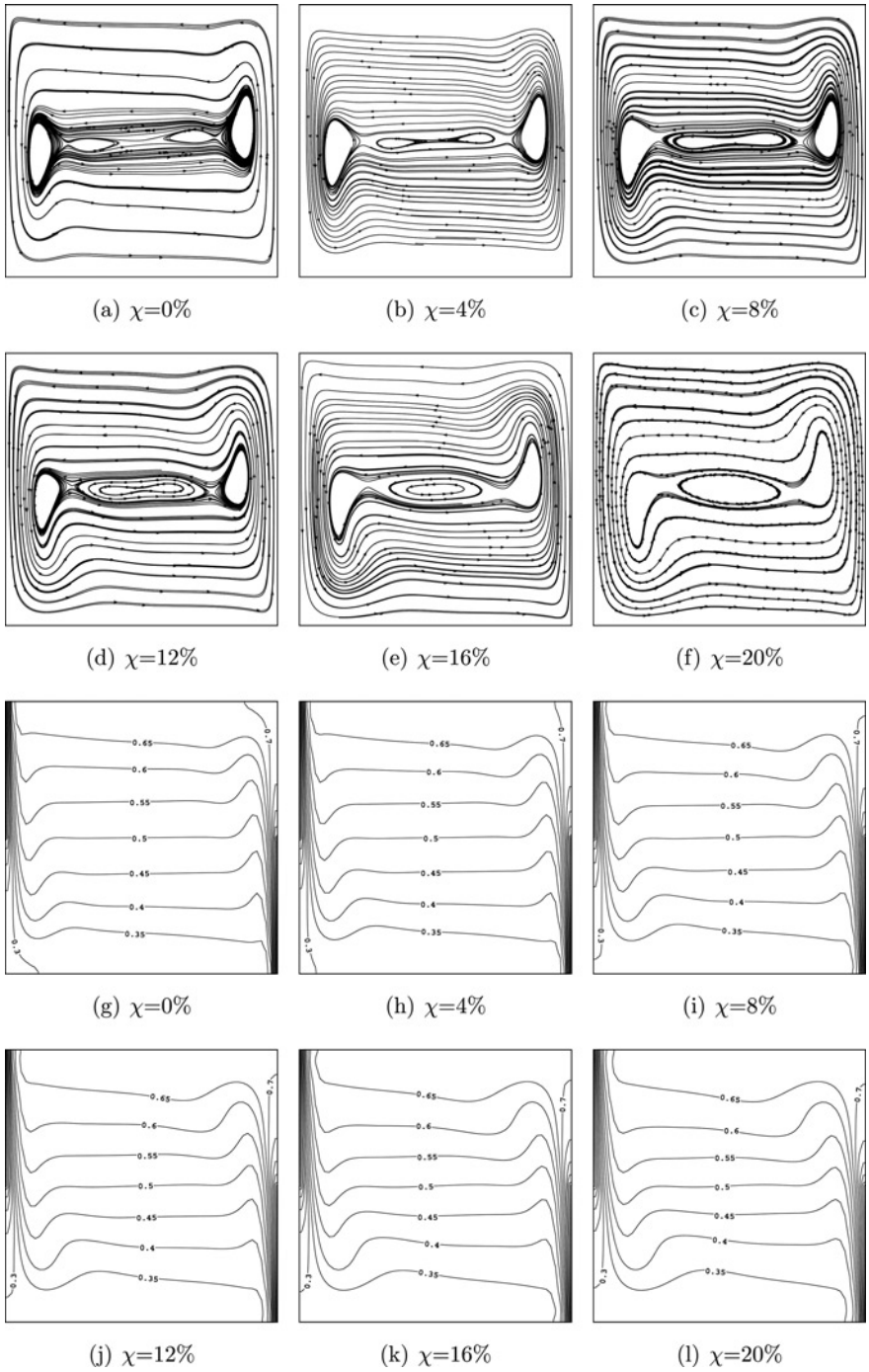

Figure 4.
Streamlines and isotherms for Case I and $Gr = 10^6$

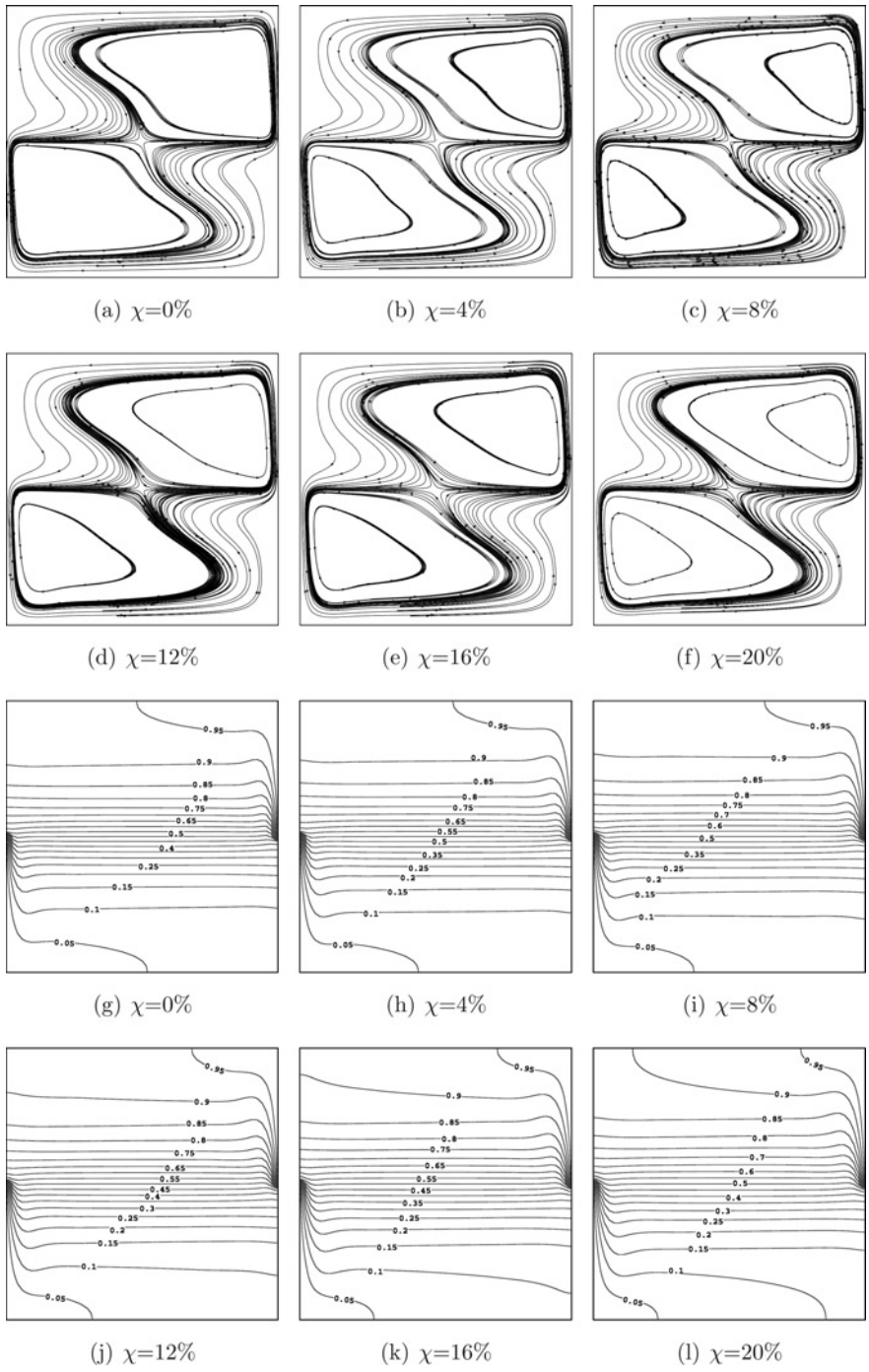

Figure 5.
Streamlines and isotherms for Case II and $Gr = 10^6$

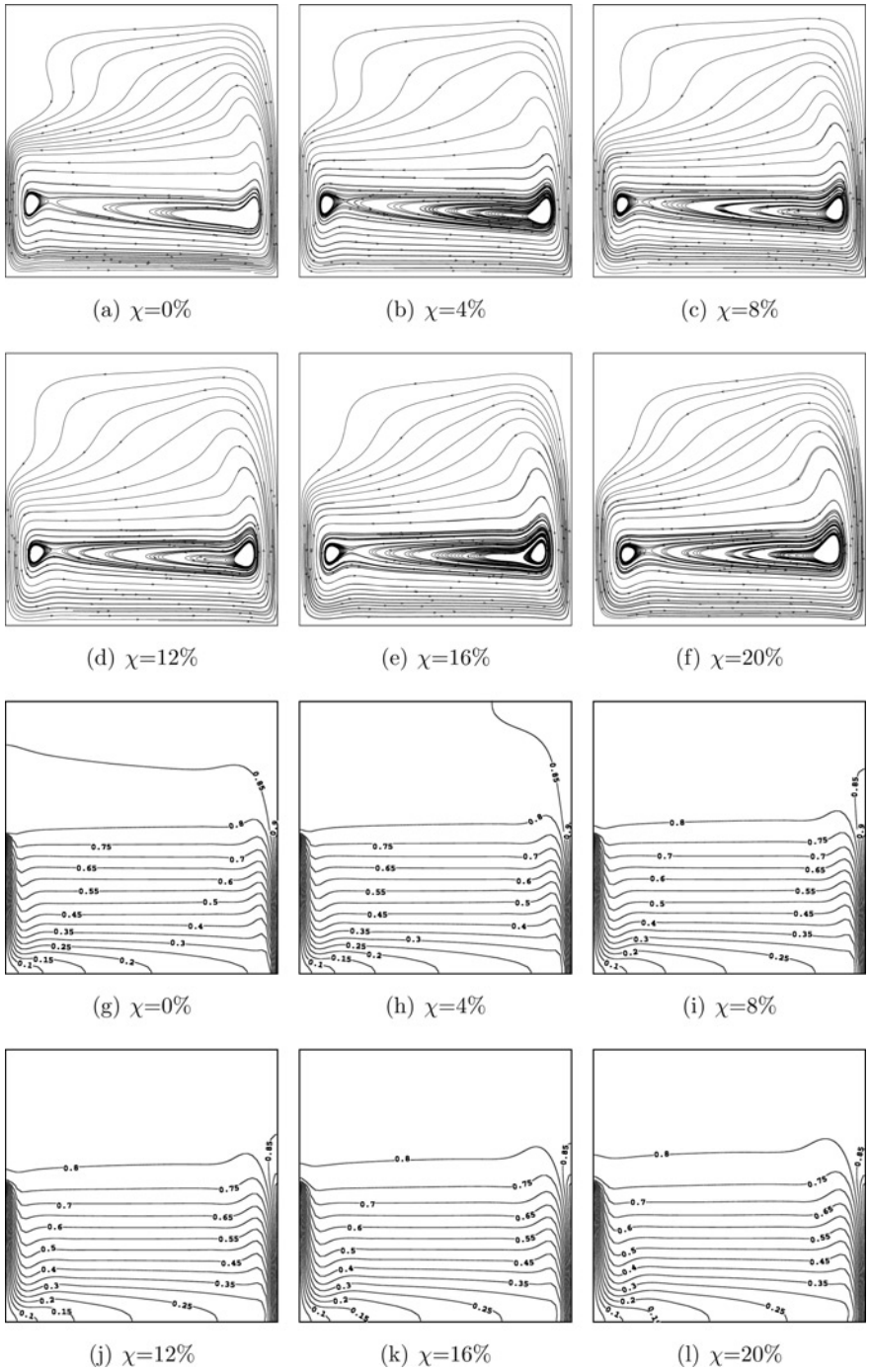

Figure 6.
Streamlines and isotherms for Case III and $Gr = 10^6$

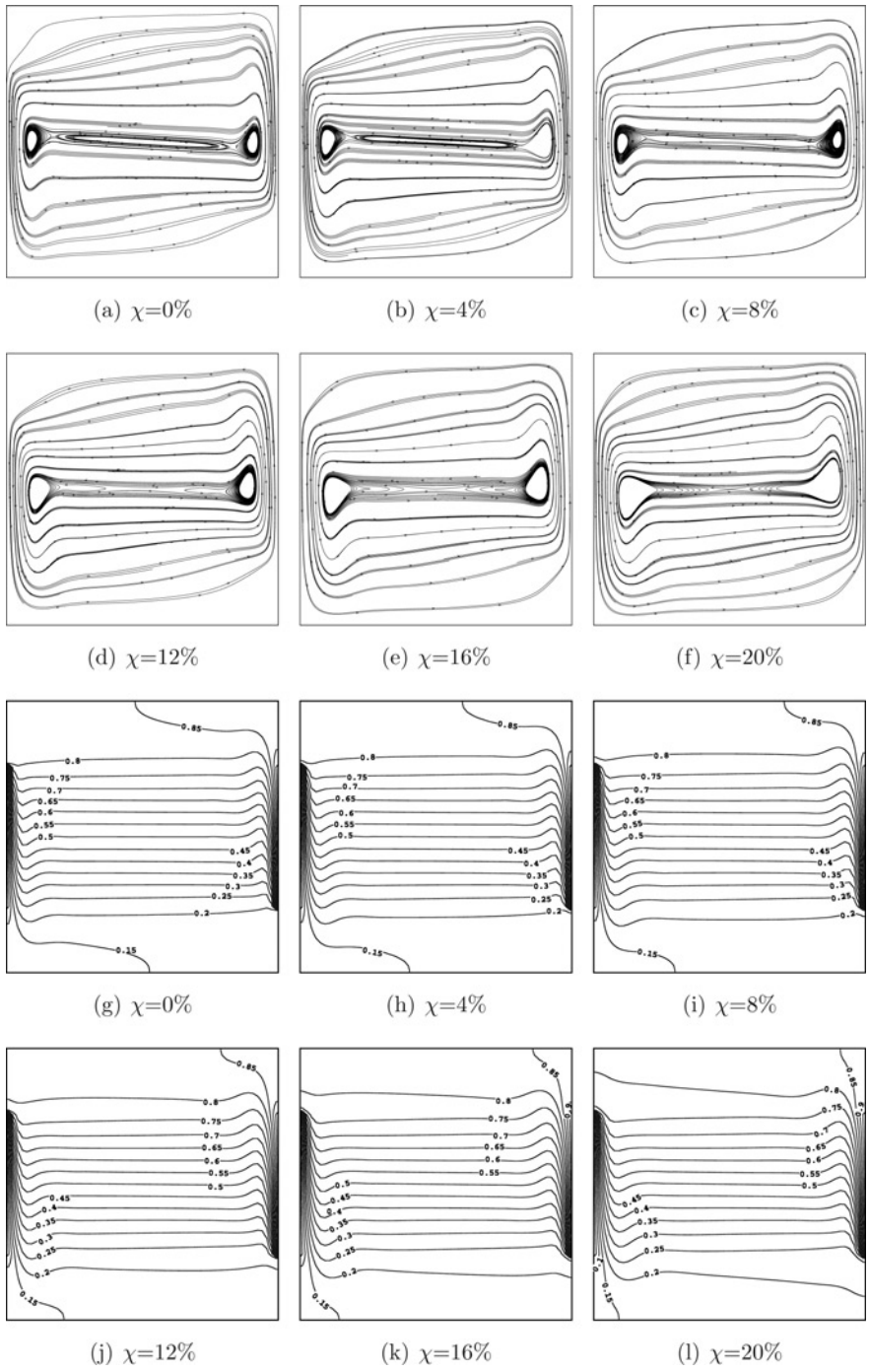

Figure 7.
Streamlines and isotherms for Case IV and $Gr = 10^6$

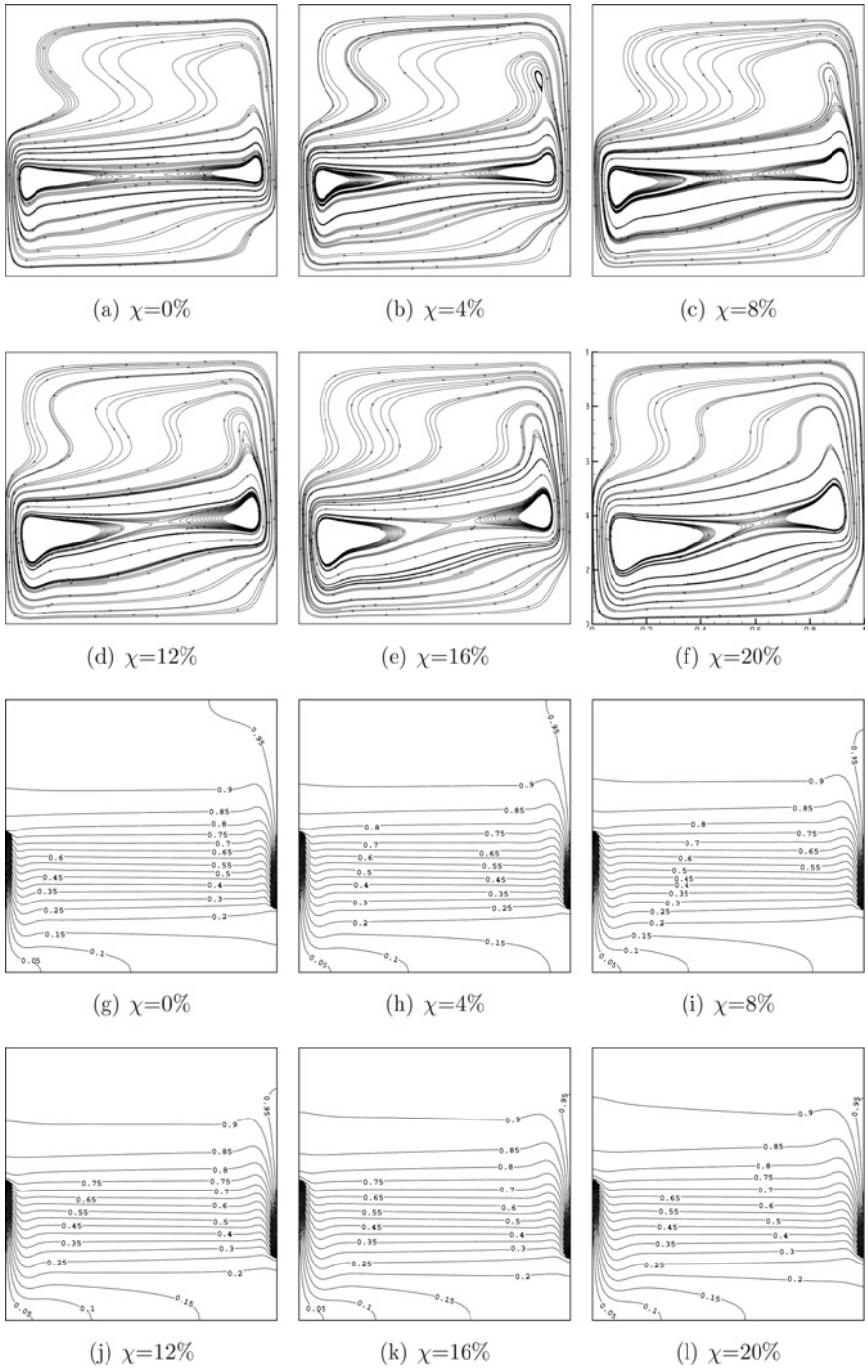

Figure 8.
Streamlines and isotherms for Case V and $Gr = 10^6$

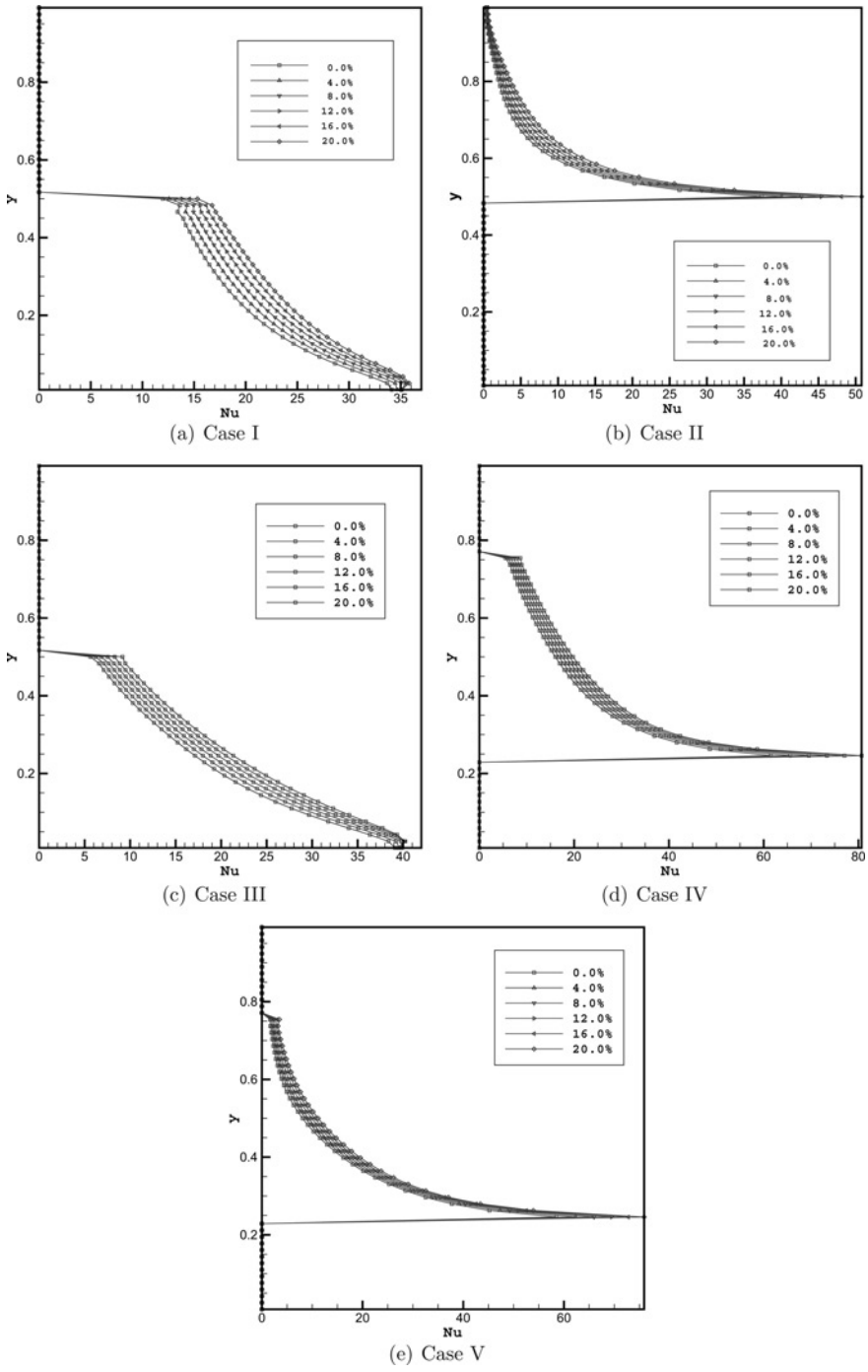

Figure 9.
Local Nusselt Number at Hot Wall for $Gr = 10^6$

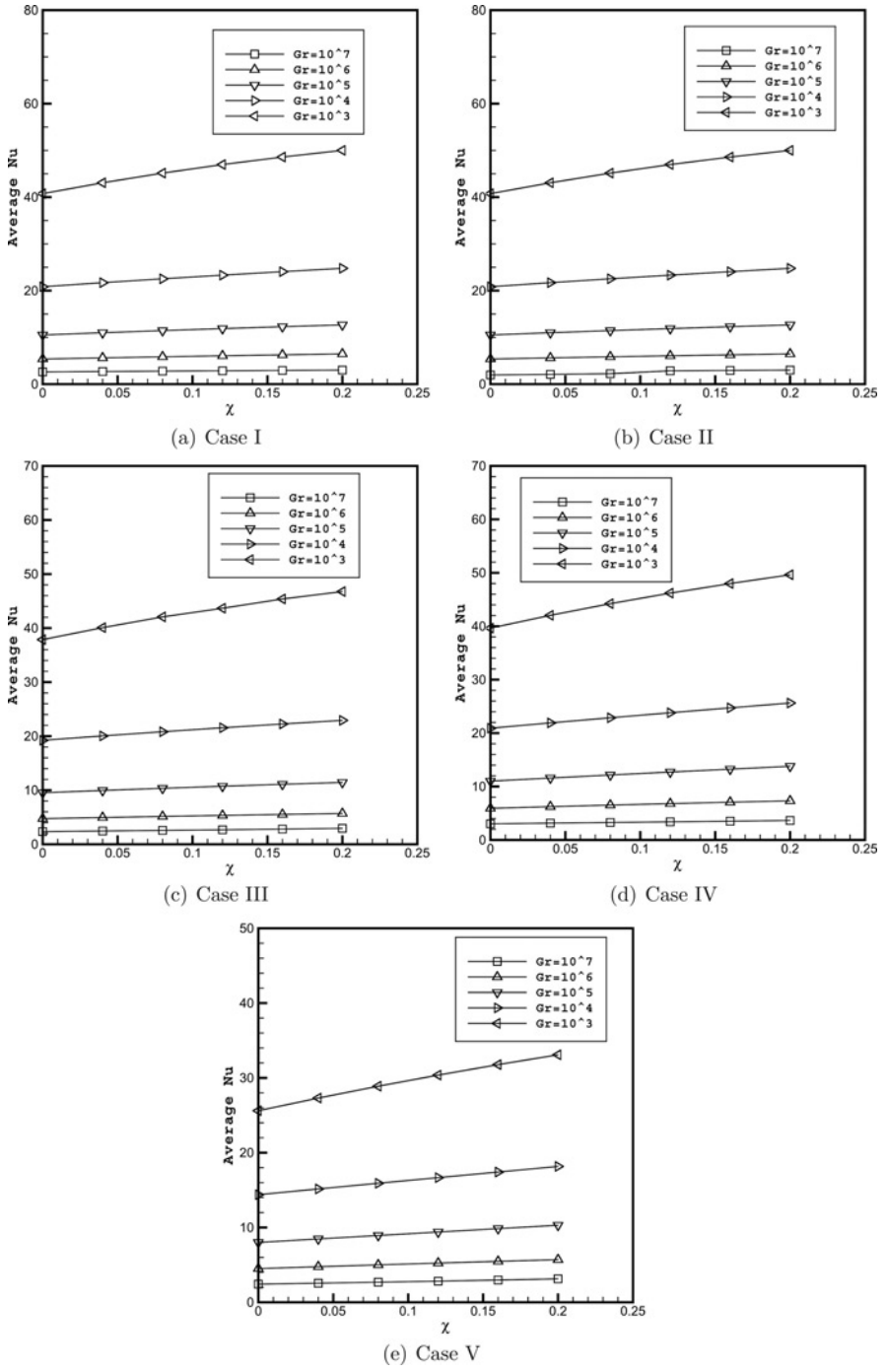

Figure 10.
Average Nusselt Number at Hot Wall for five cases

Table III.
Comparison of average Nusselt number ($\overline{Nu}$) for three cases and various solid volume fractions

Gr	A ($\chi = 0\%$)	B ($\chi = 4\%$)	%change[a]	C ($\chi = 8\%$)	%change[b]	D ($\chi = 12\%$)	%change[c]	E ($\chi = 16\%$)	%change[d]	F ($\chi = 20\%$)	%change[e]
(a) Case I											
10^3	2.61	2.71	3.49	2.79	6.58	2.86	9.39	2.93	12.19	3.02	15.42
10^4	5.39	5.63	4.45	5.85	8.69	6.07	12.73	6.28	16.57	6.47	20.20
10^5	10.52	11.00	4.54	11.45	8.85	11.88	12.93	12.29	16.79	12.67	20.46
10^6	20.84	21.71	4.17	22.54	8.12	23.32	11.86	24.06	15.43	24.78	18.87
10^7	40.74	43.07	5.71	45.14	10.79	46.97	15.28	48.59	19.24	50.01	22.74
(b) Case II											
10^3	2.34	2.45	4.74	2.56	9.48	2.68	14.37	2.80	19.69	2.95	25.80
10^4	4.73	4.94	4.44	5.14	8.65	5.33	12.66	5.51	16.48	5.69	20.14
10^5	9.52	9.95	4.46	10.35	8.68	10.73	12.66	11.09	16.43	11.43	20.01
10^6	19.23	20.04	4.23	20.82	8.25	21.55	12.07	22.25	15.71	22.92	19.18
10^7	37.86	40.08	5.85	42.07	11.09	43.66	15.31	45.38	19.84	46.75	23.46
Gr	A ($\chi = 0\%$)	B ($\chi = 4\%$)	%increase[a]	C ($\chi = 8\%$)	%increase[b]	D ($\chi = 12\%$)	%increase[c]	E ($\chi = 16\%$)	%increase[d]	F ($\chi = 20\%$)	%increase[e]
(c) Case III											
10^3	2.34	2.45	4.74	2.56	9.48	2.68	14.37	2.80	19.69	2.95	25.80
10^4	4.73	4.94	4.44	5.14	8.65	5.33	12.66	5.51	16.48	5.69	20.14
10^5	9.52	9.95	4.46	10.35	8.68	10.73	12.66	11.09	16.43	11.43	20.01
10^6	19.23	20.04	4.23	20.82	8.25	21.55	12.07	22.25	15.71	22.92	19.18
10^7	37.86	40.08	5.85	42.07	11.09	43.66	15.31	45.38	19.84	46.75	23.46
(d) Case IV											
10^3	3.02	3.15	4.31	3.27	8.34	3.39	12.25	3.51	16.26	3.64	20.76
10^4	6.22	6.52	4.70	6.80	9.19	7.06	13.46	7.31	17.5		
10^5	11.59	12.16	4.88	12.71	9.66	13.25	14.34	13.79	18.93		
10^6	20.91	21.91	4.74	22.87	9.34	23.81	13.81	24.72	18.21	25.63	22.54
10^7	39.65	42.04	6.02	44.22	11.52	46.19	16.50	47.99	21.03	49.63	25.17
(e) Case V											
10^3	2.42	2.55	5.42	2.69	10.85	2.82	16.47	2.97	22.48	3.13	29.26
10^4	4.50	4.76	5.63	5.00	11.10	5.24	16.39	5.47	21.53	5.70	26.51
10^5	8.00	8.47	5.85	8.93	11.63	9.39	17.38	9.85	23.06	10.30	28.71
10^6	14.38	15.15	15.91	16.66	17.41	18.16					
10^7	25.61	27.30	6.59	28.88	12.77	30.37	18.18	31.77	24.05	33.09	29.18

Notes: [a]$((B-A)/A) \times 100$; [b]$((C-A)/A) \times 100$; [c]$((D-A)/A) \times 100$; [d]$((E-A)/A) \times 100$; [e]$((F-A)/A) \times 100$

In Case V, the effect of solid volume fraction on the streamlines and isotherms $Gr = 10^6$ is shown in Figure 8. With the increase in χ, the strength of the vortices on the vertical walls increases and they grow bigger in size. The isotherm patterns show the formation of boundary layer at $y = 0.25$ on the hot wall and at $y = 0.5$ on the cold wall.

6.2 Local Nusselt number distribution

The local Nusselt number on the hot wall calculated from Equation (14) is shown in Figure 9 for the five cases. In all the cases, *Nu* increases with χ. However, the increase is substantial in Cases I (Figure 9(a)) and III (Figure 9(b)), whereas in other cases, the increase is not appreciable. It is to be noted that because of the partial adiabatic wall, there is a sharp increase or decrease of the Nusselt number.

6.3 Overall heat transfer

The average Nusselt number ($\overline{Nu}$) for the five cases and different *Gr* are calculated using Equation 16 and are presented in Figure 10. For Case I (Figure 10(a)), the hot wall is located at the bottom and the heat transfer is very high. With increase in χ, $\overline{Nu}$ also increases. Similar trend is obtained for Case III (Figure 10(c)) and Case IV (Figure 10(d)) where the hot wall is either located at the bottom or at the middle directly facing the cold wall. However, for Case II (Figure 10b)), the hot wall is located at the top and the heat transfer is minimum. A little improved situation is observed for Case V (Figure 10(e)) where the hot wall is at the middle and the cold wall is at the bottom. Since the distance is more, the resistance to heat transfer is more and $\overline{Nu}$ is less. In all the cases, $\overline{Nu}$ increases with χ.

The increases of $\overline{Nu}$ with *Gr* and χ for five cases are shown in Table III. For Case I, as χ is increased to 20 per cent, $\overline{Nu}$ is increased by 15 per cent for $Gr = 10^3$. For $Gr = 10^7$, the increment is by 22.7 per cent. For Case III and Case IV, these values are 25.8, 23.5 per cent and 21, 25 per cent, respectively. For Case V, they are not very far, being 29 and 29 per cent, respectively. However, the poor performance of Case II is significantly augmented by the introduction of more nanoparticles as the increment is 38 and 44.5 per cent for $Gr = 10^3$ and 10^7, χ being equal to 20 per cent.

7. Heat transfer correlations

The numerically calculated heat transfer results are correlated for the natural convection of five different cases. For each case, 105 numerical data are generated, encompassing the range of parameters $0 \leq \chi \leq 20$ per cent, $10^3 \leq Gr \leq 10^7$. A correlation for $\overline{Nu}$, having a correlation coefficient of 0.99 and an error band of ± 2 per cent is evolved for Cases I, III, IV and V. However, for Case II, the error band obtained is

Case	*a*	*b*	*c*	*d*
1	0.286	1.157	0.835	0.299
2	1	0.666	0.753	0.162
3	0.253	1.118	0.838	0.304
4	0.442	0.97	0.877	0.281
5	0.532	0.786	0.923	0.255

Table IV.
Constant *a*, *b*, *c* and *d* (Equation (17))

±10 per cent. It can be shown that the average Nusselt number is correlated as a function of χ and Gr according to the following equation.

$$\overline{Nu} = a * (b + \chi^c) Gr^d \tag{17}$$

Table IV shows the constants a, b, c, d for the five cases.

8. Conclusions

This study has been concerned with the numerical modeling of natural convection heat transfer in a sqyare cavity containing nanofluid with half-active and half-insulated vertical walls. Five different cases are considered based on the position of the active walls. The governing parameters are Gr and χ.

In view of the results obtained and discussed, the following findings may be summarized.

- The nanoparticles when immersed in a fluid are capable of increasing the heat transfer capacity of the base fluid. As solid volume fraction increases, the effect is more pronounced.
- Heat transfer is high for Cases I, III and IV. The heat transfer in Case II is minimum compared to other cases.
- The percentage increase in $\overline{Nu}$ with χ is high for Cases II and V than Cases I, III and IV.
- The percentage increase in $\overline{Nu}$ with Gr is high for Cases I, III and IV than Cases II and V.

References

Brinkman, H.C. (1952), "The viscosity of concentrated suspensions and solutions", *Journal of Chemistry Physics*, Vol. 20, pp. 571-81.

Chein, R. and Huang, G. (2005), "Analysis of microchannel heat sink performance using nanofluids", *Applied Thermal Engineering*, Vol. 25, pp. 3104-14.

de Vahl Davis, G. (1983), "Natural convection of air in a square cavity: a benchmark solution", *International Journal for Numerical Methods in Fluids*, Vol. 3, pp. 249-64.

Eastman, J.A., Choi, S.U.S., Li, S., Yu, W. and Thompson, L.J. (2001), "Anamolously increased effective thermal conductivities of ethylene glycol-based nanofluids containing copper nanoparticles", *Physics Letters Applied*, Vol. 78 No. 6, pp. 718-20.

Fusegi, T., Kuwahara, K. and Farouk, B. (1991), "A numerical study of three-dimensional natural convection in a differentially heated cubic enclosure", *International Journal of Heat and Mass Transfer*, Vol. 34 No. 6, pp. 1543-57.

Ghia, U., Ghia, K.N. and Shin, C.T. (1982), "High re solutions for incompressible flow using the Navier–Stokes equations and multigrid method", *Journal of Computational Physics*, Vol. 48, pp. 387-411.

Ha, M.Y. and Jung, M.J. (2000), "A numerical study of three-dimensional conjugate heat transfer of natural convection and conduction in a differentially heated cubic enclosure with a heatgenerating cubic conducting body", *International Journal of Heat and Mass Transfer*, Vol. 43, pp. 4229-48.

Hadjisophocleous, G.V., Sousa, A.C.M. and Venart, J.E.S. (1998), "Predicting the transient natural convection in enclosures of arbitrary geometry using a nonorthogonal numerical model", *Numerical Heat Transfer: Part A*, Vol. 13, pp. 373-92.

Hamilton, R.L. and Crosser, O.K. (1962), "Thermal conductivity of heterogeneous two-component systems", *Induatrial and Engineering Chemistry: Fundamentals*, Vol. 1, pp. 182-91.

Hayase, T., Humphrey, J.A.C. and Greif, R. (1990), "A consistently formulated QUICK scheme for fast and stable convergence using finite-volume iterative calculation procedures", *Journal of Computational Physics*, Vol. 98, pp. 108-18.

Khanafer, K., Vafai, K. and Lightstone, M. (2003), "Buoyancy driven heat transfer enhancement in a two-dimensional enclosure utilizing nanofluids", *International Journal of Heat and Mass Transfer*, Vol. 46, pp. 3639-53.

Koo, J. and Kleinstreuer, C. (2005), "Laminar nanofluid flow in microheat-sinks", *International Journal of Heat and Mass Transfer*, Vol. 48, pp. 2652-61.

Markatos, N.C. and Pericleous, K.A. (1984), "Laminar and turbulent natural convection in an enclosed cavity", *International Journal of Heat and Mass Transfer*, Vol. 27 No. 5, pp. 755-72.

Maxwell, J.C. (1904), *A Treatise on Electricity and Magnetism*, 2nd ed., Oxford University Press, Oxford, pp. 435-41.

Patankar, S.V. (1980), *Numerical Heat Transfer and Fluid Flow*, Hemisphere Publication Company, New York, NY, ISBN 0-07-048740-5.

Santra, A.K., Sen, S. and Chakraborty, N. (2004), "Analysis of laminar natural convection in a square cavity using nanofluid", 31st National Conference on FMFP, Jadavpur University Kolkata, pp. 240-8.

Tiwari, R.K. and Das, M.K. (2007), "Heat transfer augmentation in two-sided lid-driven differentially heated square cavity utilizing nanofluids", *International Journal of Heat and Mass Transfer*, Vol. 50, pp. 2002-18. doi:10.1016/j.ijheatmasstransfer.2006.09.034.

Valencia, A. and Frederick, R.L. (1989), "Heat transfer in square cavities with partially active walls", *International Journal of Heat and Mass Transfer*, Vol. 32, pp. 1567-74.

Van Doormaal, J.P. and Raithby, G.D. (1984), "Enhancements of the SIMPLE method for predicting incompressible fluid flows", *Numerical Heat Transfer: Part A*, Vol. 7, pp. 147-63.

Xuan, Y. and Li, Q. (1999), *Report of Nanjing University of Sciences and Technology*, in Chinese.

Xuan, Y. and Li, Q. (2003), "Investigation on convective heat transfer and flow features of nanofluids", *ASME Journal of Heat Transfer*, Vol. 125, pp. 151-5.

About the authors

Manab Kumar Das was formerly an Associate Professor at the Indian Institute of Technology Guwahati and is currently an Associate Professor in the Department of Mechanical Engineering, Indian Institute of Technology Kharagpur, India. Manab Kumar Das is the corresponding author and can be contacted at: manab@mech.iitkgp.ernet.in

Pravin Shridhar Ohal was formerly a graduate student at the Indian Institute of Technology Guwahati and currently is with Tata Motors, Pune, India.